



Published in final edited form as:

*J Bone Miner Metab.* 2018 November ; 36(6): 661–667. doi:10.1007/s00774-017-0887-7.

## Increased calcium uptake and improved trabecular bone properties in intestinal alkaline phosphatase knockout mice

Lucas R. Brun<sup>1,2</sup>, M. Lombarte<sup>1,2</sup>, S. Roma<sup>3</sup>, F. Perez<sup>3</sup>, J. L. Millán<sup>4</sup>, and A. Rigalli<sup>1,2,5</sup>

<sup>1</sup>Bone Biology Laboratory, Cátedra de Química Biológica, Facultad de Ciencias Médicas, School of Medicine, Rosario National University, Santa Fe 3100, 2000 Rosario, Argentina

<sup>2</sup>National Council of Scientific and Technical Research (CONICET), Rosario, Argentina

<sup>3</sup>Histology and Embryology Department, School of Medicine, Rosario National University, Rosario, Argentina

<sup>4</sup>Sanford Burnham Prebys Medical Discovery Institute, La Jolla, USA

<sup>5</sup>Rosario National University Research Council, Rosario, Argentina

### Abstract

Previous studies have demonstrated a negative correlation between intestinal alkaline phosphatase (IAP) activity and calcium (Ca) absorption in the gut, as IAP acts as a protective mechanism inhibiting high Ca entry into enterocytes, preventing Ca overload. Here we evaluated Ca absorption and bone properties in knockout mice (KO) completely devoid of duodenal IAP (*Akp3*<sup>-/-</sup> mice). Female C57BL/6 control mice (WT,  $n = 7$ ) and KO mice ( $n = 10$ ) were used to determine Ca absorption in vivo and by in situ isolated duodenal loops followed by histomorphometric analysis of duodenal villi and crypts. Bone mineral density, morphometry, histomorphometry and trabecular connectivity and biomechanical properties were measured on bones. We observed mild atrophy of the villi with lower absorption surface and a significantly higher Ca uptake in KO mice. While no changes were seen in cortical bone, we found better trabecular connectivity and biomechanical properties in the femurs of KO mice compared to WT mice. Our data indicate that IAP KO mice display higher intestinal Ca uptake, which over time appears to correlate with a positive effect on the biomechanical properties of trabecular bone.

### Keywords

Intestinal alkaline phosphatase; Bone properties; Calcium absorption

### Introduction

Calcium (Ca) is essential not only for calcified tissue formation, but also for muscle contraction, exocrine secretion, regulation of enzyme activity, excitability and permeability

---

Lucas R. Brun lbrun@unr.edu.ar

Compliance with ethical standards

**Conflict of interest** The authors report no conflict of interest.

of the plasma membrane, neurotransmission and signal transduction pathways. Ca homeostasis is regulated by changes in Ca absorption, bone remodeling and urinary Ca excretion, which are subject to hormonal regulation by para-thyroid hormone, calcitonin and vitamin D [1]. In humans, net Ca absorption is not higher than 500–600 mg/day, even when Ca intake goes above 1000 mg/day [2]. A similar situation has been observed in rats [3], and a minute-to-minute regulatory mechanism of Ca uptake dependent of Ca luminal concentration by intestinal alkaline phosphatase (IAP) activity has been proposed [4].

IAP is a brush border enzyme that controls a rate-limiting step in fatty acid absorption in the gut through a yet unclear mechanism [5], and is crucial for the maintenance of the gut microbiota and gut barrier function via its ability to hydrolyze ATP and bacterial lipopolysaccharides (LPS), two potent pro-inflammatory molecules [6, 7]. Two genes have been described in the rat that encode distinct IAP isozymes: IAP I located along the whole intestine and IAP II, whose expression is restricted to the duodenum [8]. In mice, three genes are expressed in the gut: *Akp3* in the duodenum; *Akp5* along the entire length of the gut and *Akp6* with higher expression in the distal gut [9]. Previous studies have shown a relationship between IAP activity and Ca absorption [10–12], and a stimulating effect of Ca on the activity of IAP in the rat duodenum was observed [3]. In vivo, the inhibition of IAP with L-phenylalanine (Phe) increases the percentage of Ca absorption. This fact is more evident in rats that are fed with a low-Ca diet [3]. Also, it has been demonstrated that IAP modifies the luminal pH as a function of enzyme concentration and Ca luminal content [4]. In addition, a decrease in pH occurred simultaneously with a decrease in Ca absorption [4]. This decrease in pH mediated by IAP activity as a function of Ca luminal content would inhibit the TRPV6 channels [13–15]. Therefore, a role of IAP in the regulation of intestinal Ca absorption by luminal Ca content is hypothesized in which IAP would provide a protective mechanism to inhibit high Ca entry into enterocytes. Here, we tested the hypothesis that mice null for duodenal IAP would display constitutively high Ca absorption and better bone properties.

## Materials and methods

### Animals

Four-month-old female C57BL/6 control mice (WT,  $n = 7$ ) and sibling duodenal alkaline phosphatase knockout mice (*Akp3*<sup>-/-</sup>) [5] (KO,  $n = 10$ ) were used. Mice were housed in a room with 12-h light and dark periods, and constant temperature of  $24 \pm 1$  °C. The body weight and food intake were recorded weekly. All the experiments were conducted in accordance with international guidelines for animal care [16] and have been approved by the Bioethics Committee of School of Medicine, Rosario National University, Argentina. Animals were fed according to American Institute of Nutrition recommendations [17].

### In vivo Ca absorption, calcemia and phosphatemia determinations

The animals were placed in individual metabolic cages for 24 h. Urine and feces were collected and the amount of food eaten was measured. The amount of Ca in food, feces and urine were determined by atomic absorption spectroscopy (Arolab MK II, Buenos Aires, Argentina). Calciuria and 24-h urinary volume were used to calculate 24-h urinary Ca

excretion (mg/24-h). The 24-h Ca intake and 24-h fecal Ca were calculated. The net Ca absorption for each animal was calculated as 24-h Ca intake—24 h fecal Ca and the Ca retention was calculated as 24-h Ca intake—24-h fecal Ca—24-h urinary Ca excretion [3].

In addition, calcemia (mg/dl) and phosphatemia (mg/dl) were spectrophotometrically measured on a Perkin Elmer Lambda 11 (Perkin Elmer Corporation Norwalk, CT, USA) with commercial kits (Ca Color and Fosfatemia UV, Wiener Lab, Rosario, Argentina).

### Ca absorption in isolated duodenal loops

WT and KO mice were anesthetized intraperitoneally with urethane (120 mg/100 g body weight) and kept in thermostated stretchers. During the experiment, the room temperature was maintained between 21 and 22 °C and the animal body temperature at  $35 \pm 1$  °C. Two centimeters of the duodenum distal to the pylorus were isolated and a catheter was placed at the distal end [18]. Two hundred  $\mu$ l of filling solution (1 mM Tris, 1 mM  $MgCl_2$ , 160 mM glucose, 50 mM Ca, pH 9) were introduced in the isolated duodenal loop through the catheter. Samples of the duodenum filling solution were obtained immediately after filling ( $t = 0$ ) and after 20 min of incubation. The difference between Ca in filling solution at  $t = 0$  and after 20 min was used to calculate the percentage of Ca absorption. The Ca concentration was measured by atomic absorption spectroscopy (Arolab MK II, Buenos Aires, Argentina).

### Duodenal histomorphometry

Samples of duodenum were fixed in 10% phosphate buffered formaldehyde before paraffin embedding. Five- $\mu$ m longitudinal sections were cut and 4 sections per mouse (WT,  $n = 7$  and KO,  $n = 10$ ) were stained with hematoxylin and eosin to be analyzed. The slides were examined by a pathologist using a light microscope (Mikoba 320, China) to evaluate the morphological characteristics of duodenal epithelium. In addition, digital images (200–600 $\times$ ) were obtained (Olympus SP-350, China) and a histomorphometry analysis of duodenal villus and crypts were performed with Image J 1.48 software (NIH, Maryland, USA). In each slide, all villi that appear cut along the long axis of villi were measured. On each duodenal villus, the height, the diameter and the perimeter were determined. Also, the total perimeter of the whole duodenal villus in each slide was measured. On each duodenal crypt, the diameter, the area of the crypts, the area of cells and the height of the crypts cells were measured.

### Bone analysis

**BMD, morphometry and histomorphometry**—Bone mineral density (BMD, mg  $Ca/cm^2$ ) was determined on left tibias using X-ray absorption measurement (Work Ray 70 kV, Workman SRL, Argentina) simultaneously with an aluminum step wedge, which was previously calibrated with known Ca concentrations [19]. The BMD was determined at the same anatomical location later used for histomorphometric measurements with Image J 1.48 software.

For morphometric analysis of bone, X-ray images were used. Total length (mm), total diameter (mm) and cortical bone thickness (mm) at mid-diaphysis were measured with Image J 1.48 software.

The proximal epiphysis of the right tibias were fixed in 10% phosphate buffered formaldehyde and decalcified in 10% EDTA before paraffin embedding. Five- $\mu\text{m}$  longitudinal sections were stained with hematoxylin and eosin and slides were examined using a light microscope (Mikoba 320, China). Digital images were obtained at  $100\times$  magnification (Olympus SP-350, China). Analyses were performed in a  $0.6\text{ mm}^2$  area at 0.1 mm from the growth plate metaphyseal junction. The following measurements were performed with Image J 1.48 software as described by Parfitt et al. [20]: (1) total tissue volume, TV ( $\text{mm}^2$ ); (2) trabecular bone volume, BV ( $\text{mm}^2$ ); and (3) trabecular bone surface, BS (mm). With these values, histomorphometrical parameters were calculated: (1) bone volume, BV/TV (%) =  $[\text{BV} \times 100 / \text{TV}]$ ; (2) trabecular thickness, Tb.Th (mm) =  $[2 / (\text{BS} / \text{BV})]$ ; (3) trabecular number, Tb.N ( $\text{mm}^{-1}$ ) =  $[(\text{BV} / \text{TV}) / (\text{Tb.Th})]$ ; and (4) trabecular separation, Tb.Sp (mm) =  $[(1 / \text{Tb.N}) - \text{Tb.Th}]$ . In addition, an analysis of trabecular connectivity was calculated from the characteristics of the skeletonized image of the trabecular structure on the same digital images (Fig. 1). The following parameters were measured (ImageJ 1.48 software): total number of nodes (Nd), number of node-to-node branches (NNd), number of node-to-termini branches (NNdTm), number of trees ( $T$ ), number of terminals (Tm), and number of branches with two terminals (NTm). With these parameters, we calculated the interconnectivity parameters: interconnectivity index  $[\text{ICI} = \text{Nd} \times \text{NNd} / T \times (\text{NNdTm} + 1)]$ ; node-to-termini ratio  $[\text{R} = \text{Nd} / \text{Tm}]$ ; mean size of branches  $[\text{Dist} (\text{mm}) = \text{branches size} / (\text{NNdTm} + \text{NNd} + \text{NTm})]$ ; and the new interconnectivity index  $[\text{NDX} (\%/ \text{mm}) = (\text{R} \times \text{NNd} \times (\text{BV} / \text{TV}) \times \text{Tb.Th}) / ((\text{NTm} + \text{NNdTm}) \times \text{Dist} \times \text{Tb.Sp})]$  [19, 21]. The higher ICI, R and NDX and the lower NTm indicates more connectivity among trabeculas.

**Mechanical testing**—Femurs were stored at  $-20\text{ }^\circ\text{C}$  wrapped in saline soaked gauze until tested, and were thawed at  $37\text{ }^\circ\text{C}$ . Cortical bone strength at the femoral mid-diaphysis was determined using three-point bending test [22]. The two-bar distance for the three-point bending test was 7 mm. In addition, femoral neck fracture was carried out to evaluate trabecular bone. The femur, cut at 1 cm from the proximal diaphysis, was placed in stable three-point (diaphysis, femoral head and greater trochanter) in contact with a flat surface [23] and the fracture was performed with a flat surface of  $7.07\text{ mm}^2$ . Mechanical testing was performed on a machine with a 300 N load cell with 0.01 Newton of discrimination and an accuracy of  $10\text{ }\mu\text{m}$  in displacements. For both tests, the speed, which was  $0.01\text{ mm/s}$ , was monitored with a computer. Load vs. displacement plots were recorded by software Biomedical Data Acquisition Suite 1.0 (Argentina, 2011). The software data acquisition rate was 10 Hz. Ultimate load (N) was defined as the highest load and the fracture load (N) was recorded just before the first decline in load. The stiffness (N/mm) was determined as the slope of the linear portion of the load vs. displacement curve. Absorbed energy (mJ) was defined as the area under the curve until the fracture load point.

**Statistical analysis**—Data were expressed as mean  $\pm$  SEM. Student's *t* test was performed to compare WT and KO mice. Differences were considered significant if  $p < 0.05$ . Statistical analyses were performed using the software R 3.2.2 [24].

## Results

### In vivo Ca absorption, calcium and phosphate in serum

No significant differences between groups were found in serum Ca and phosphate. No statistical difference was found in urinary calcium, net Ca absorption or Ca retention (Table 1).

### Duodenal morphological analysis

WT mice showed that villi are regular to each other, thin and elongated, covered by a single layer of epithelium, with a villous to crypt ratio  $\sim 4:1$ . The lamina propria shows a regular amount of cells (Fig. 2, left). On the other hand, in KO mice, villi showed mild atrophy, with a slight decrease in height and widening (Fig. 2, right). The lamina propria exhibited poor cellularity. Crypts showed no differences between groups.

According to histopathological analysis, a significant increase in villous diameter and a reduced villous height and perimeter were found in KO mice compared to WT mice. In addition, a diminished total perimeter was observed in KO mice (Table 2) corresponding to a decrease in surface epithelium in which the Ca absorption occurs. Histomorphometric analysis of the crypts showed no significant difference between the two groups (Table 2).

### Ca absorption in isolated duodenal loops

Although no significant differences between groups was found, a higher percentage of Ca absorption was observed in KO mice (WT =  $31.47 \pm 6.05\%$ , KO =  $42.85 \pm 8.22\%$ ;  $p > 0.05$ ) compared to WT controls. When the Ca absorption data were corrected for the absorptive surface according to duodenal morphological analysis, a significantly higher percentage of Ca absorption was found in KO mice ( $16.17 \pm 3.10\%$ ) compared to WT mice ( $8.89 \pm 1.71\%$ ) (Fig. 3, Student's *t* test,  $p < 0.05$ ).

### BMD, morphometry and histomorphometry

The total length, total diameter and cortical bone thickness showed no significant difference (data not shown).

The BMD showed no statistical differences between groups (Table 3). As BMD, the BV/TV showed no statistically significant difference but a substantial increase in both variables was observed in KO mice (Table 3).

The node-terminal ratio was significantly higher in the KO mice. Similarly but without reaching statistical significance due to the dispersion of data, the trabecular connectivity parameters ICI and NDX were found to be increased in the KO group. According to connectivity parameter data, the NTm—a disruption parameter—was found to be

significantly lower in KO mice. Altogether, these results suggest better trabecular connectivity in KO mice (Table 3).

### Mechanical testing

The three point bending test—which evaluates cortical bone—showed no differences between groups (fracture load = WT:  $19.48 \pm 0.48$  N, KO:  $18.12 \pm 0.45$  N; ultimate load = WT:  $20.99 \pm 0.91$  N, KO:  $19.26 \pm 0.47$  N; stiffness = WT:  $40.07 \pm 7.80$  N/mm, KO:  $31.01 \pm 3.57$  N/mm; absorbed energy = WT:  $4.76 \pm 0.77$  mJ, KO:  $3.57 \pm 0.30$  mJ).

On the other hand, the femoral neck fracture test showed significant differences between groups (Fig. 4.): fracture load = WT:  $20.66 \pm 1.96$  N, KO:  $28.71 \pm 1.69$  N; ultimate load = WT:  $20.67 \pm 1.97$  N, KO:  $28.78 \pm 1.69$  N; and absorbed energy = WT:  $3.61 \pm 0.97$  mJ, KO:  $9.36 \pm 1.37$  mJ (Student's *t* test,  $p < 0.05$ ).

No differences in body weight or food intake which could affect the bone parameters were observed (data not shown).

### Discussion

Previous studies have proposed that IAP acts in the regulatory mechanism of intestinal Ca uptake [3, 4]. In vitro and in vivo experiments using the IAP inhibitor L-phenylalanine (Phe) demonstrated an increase in Ca absorption [3, 4]. Here we used mice null for duodenal IAP (Akp3<sup>-/-</sup> mice) to assess the predicted increase in Ca absorption and expected changes in bone properties.

It has been previously demonstrated that higher Ca intake would be positive for bone metabolism. Retrospective studies in populations with different Ca intake (400–500 vs 900–1000 mg/day) throughout their lifetimes described a higher bone mass and a lower incidence of femoral and wrist fractures [25]. Studies in children have found a positive correlation between Ca intake and bone mass. The importance of Ca intake was also observed during childhood to obtain an adequate peak of bone mass [26–28]. Also, children with very low basal Ca intake (< 500 mg/day) who received extra Ca contribution showed a greater increase of BMD at the lumbar spine than controls [29, 30]. However, other authors have not found this correlation [31, 32]. This discrepancy may be partially due to the difficulty and heterogeneity of nutritional questionnaires and because the higher Ca intake comes from dairy products and, therefore, different caloric intakes could be implicated. However, the increased intake of dairy foods did not increase overall total or saturated fat intake and was not associated with excessive weight gain or increased body fat [27]. The mechanisms for a greater increase of bone mass with Ca supplementation in children and adolescents might involve the reduction of bone remodeling and stimulated osteoblasts synthesis through the increase in the production and secretion of insulin growth factor (IGF-1) [33].

Therefore, a higher Ca absorption may explain the improved biomechanical properties found in the trabecular bone of the 4-month-old KO mice used in this study. Despite higher values in KO mice in in vivo net Ca absorption and Ca retention and in Ca absorption in isolated duodenal loops, no statistical differences were found. However, when the Ca uptake was

analyzed as a function of the absorption surface, the KO mice showed significantly higher Ca uptake compared to WT mice. Accordingly, more Ca would reach the bones in the long term, which could explain the improved biomechanical properties found in KO mice. Moreover, KO mice showed mild atrophy of the epithelium and the villi were shorter and wider, which causes a decrease in the absorption surface without differences in the crypts. Previously, a normal histomorphological appearance of the intestine between KO mice and control animals has been reported. However, no morphometric analyses were performed in the mentioned study [5]. As was proposed previously, IAP acts as a protective mechanism to inhibit the entry of high Ca content into enterocytes [4], thus it can prevent an increase in intracellular Ca, which may cause cellular damage. The increase in intracellular Ca in mice devoid of IAP may be responsible for the atrophy of the epithelium found in this study. Another possible explanation for the epithelium atrophy could be an adaptive mechanism to avoid high Ca entry into enterocytes, preventing Ca overload.

Increased Ca uptake during growth in KO mice could be responsible for their better bone properties compared to WT mice. While no changes were found in cortical bone thickness or the three point bending test, improved trabecular properties were found in IAP KO mice. Despite no statistically significant differences, KO mice showed an increase of 27% in BMD and a similar increase in BV/TV was observed. In addition, a significant increase in trabecular connectivity was found. The node-termini ratio was significantly higher in KO mice and the NTm—a disruption parameter—was significantly lower in KO mice. Although not reaching statistical significance due to the dispersion of data, NDX and ICI were higher in KO mice. In accord with better bone properties in KO mice, significantly higher trabecular biomechanical parameters (fracture load, ultimate load and absorbed energy) were observed after the femoral neck fracture test. Taken together these results showed better bone quality in IAP KO mice, which could be explained by the higher Ca uptake due to IAP deficiency according to the model previously reported [4]. Given that the naturally occurring amino acid L-phenylalanine has long been known as an IAP inhibitor, an interesting relationship between high-meat protein intake and bone mass has also been described. High protein intake has been considered a risk factor for osteoporosis due to the increase in urinary Ca excretion resulting from the metabolic acidity of protein metabolism [34]. However, many epidemiological studies have shown that long-term high-protein intake increases BMD and reduces bone fracture incidence [35]. Also, low-protein intake in young healthy women depressed intestinal Ca absorption and this effect was accompanied by elevations in parathyroid hormone [36]. Therefore, high-protein intake could provide high L-phenylalanine luminal concentration which could inhibit, at least in part, IAP activity. This would lead to increased Ca uptake as was demonstrated previously after IAP inhibition with L-phenylalanine [3, 4], and here with mice null for duodenal IAP.

In conclusion, KO mice showed higher Ca uptake, which chronically appears to have a positive effect on trabecular bone properties. These results provide more evidence that IAP acts in Ca absorption regulation.

## Acknowledgements

We thank Candela Retamozo, Damián Lescano and Alexia Cornejo for the technical assistance. This work was funded by Grant from CONICET (PIP 112 201501 00619 CO).

## References

1. Norman AW (1979) Vitamin D metabolism and calcium absorption. *Am J Med* 67:989–998 [PubMed: 229729]
2. Favus MJ, Bushinsky DA, Leamann J (2006) Regulation of calcium, magnesium and phosphate metabolism. In: *Primer on the metabolic bone disease and disorders of mineral metabolism*, 6th edn. American Society for Bone and Mineral Research
3. Brun LR, Brance ML, Rigalli A (2012) Luminal calcium concentration controls intestinal calcium absorption by modification of intestinal alkaline phosphatase activity. *Br J Nutr* 108:229–233 [PubMed: 22018098]
4. Brun LR, Brance ML, Lombarte M, Lupo M, Di Loreto VE, Rigalli A (2014) Regulation of intestinal calcium absorption by luminal calcium content: role of intestinal alkaline phosphatase. *Mol Nutr Food Res* 58:1451–1546
5. Narisawa S, Huang L, Iwasaki A, Hasegawa H, Millán JL, Alpers DH (2003) Accelerated fat absorption in intestinal alkaline phosphatase knockout mice. *Mol Cell Biol* 23:7525–7530 [PubMed: 14560000]
6. Goldberg RF, Austen WG, Jr, Zhang X, Munene G, Mostafa G, Biswas S, McCormack M, Eberlin KR, Nguyen JT, Tatlidede HS, Warren HS, Narisawa S, Millán JL, Hodin RA (2008) Intestinal alkaline phosphatase is a gut mucosal defense factor maintained by enteral nutrition. *Proc Natl Acad Sci USA* 105:3551–3556 [PubMed: 18292227]
7. Malo MS, Alam SN, Mostafa G, Zeller SJ, Johnson PV, Mohammad N, Chen KT, Moss AK, Ramasamy S, Faruqui A, Hodin S, Malo PS, Ebrahimi F, Biswas B, Narisawa S, Millán JL, Warren HS, Kaplan JB, Kitts CL, Hohmann EL, Hodin RA (2010) Intestinal alkaline phosphatase preserves the normal homeostasis of gut microbiota. *Gut* 59:1476–1484 [PubMed: 20947883]
8. Xie Q, Alpers DH (2000) The two isoenzymes of rat intestinal alkaline phosphatase are products of two distinct genes. *Physiol Genom* 3:1–8
9. Narisawa S, Hoylaerts MF, Doctor KS, Fukuda MN, Alpers DH, Millán JL (2007) A novel phosphatase upregulated in Akp3 knockout mice. *Am J Physiol Gastrointest Liver Physiol* 293:G1068–G1077 [PubMed: 17901166]
10. Strom M, Krisinger J, DeLuca HF (1991) Isolation of a mRNA that encodes a putative intestinal alkaline phosphatase regulated by 1,25-dihydroxyvitamin D-3. *Biochim Biophys Acta* 1090:299–304 [PubMed: 1954251]
11. Brun LR, Traverso A, Rigalli A (2009) Aggregation and inhibition of rat intestinal alkaline phosphatase by high concentrations of calcium. Reversibility of the processes. *J Enzyme Inhib Med Chem* 24:691–696 [PubMed: 18951287]
12. Brun LR, Brance ML, Rigalli A, Puche RC (2006) Effect of calcium on rat intestinal alkaline phosphatase activity and molecular aggregation. *J Enzyme Inhib Med Chem* 21:757–763 [PubMed: 17252950]
13. Peng J, Brown EM, Hediger MA (2003) Epithelial Ca<sup>++</sup> entry channels: transcellular Ca<sup>++</sup> transport and beyond. *J Physiol* 551:729–740 [PubMed: 12869611]
14. Hoenderop JG, van der Kemp AW, Hartog A, van de Graaf SF, van Os CH, Willems PH, Bindels RJ (1999) Molecular identification of the apical Ca<sup>2+</sup> channel in 1, 25-dihydroxyvitamin D3-responsive epithelia. *J Biol Chem* 274:8375–8378 [PubMed: 10085067]
15. Vennekens R, Prenen J, Hoenderop JG, Bindels RJ, Droogmans G, Nilius B (2001) Modulation of the epithelial Ca<sup>2+</sup> channel ECaC by extracellular pH. *Pflugers Arch* 442:237–242 [PubMed: 11417220]
16. Canadian Council on Animal Care Guidelines (1998). *Guide to the care and use of experimental animal*, 2nd edn

17. Reeves PG, Nielsen FH, Fahey GC, Jr (1993) AIN-93 purified diets for laboratory rodents: final report of the American Institute of Nutrition ad hoc writing committee on the reformulation of the AIN-76A rodent diet. *J Nutr* 123:1939–1951 [PubMed: 8229312]
18. Brance ML, Brun LR, Rigalli A (2009) In situ isolation of the intestinal loop. In: Rigalli A, Di Loreto V (eds) *Experimental surgical models in the Laboratory Rat*, 1st edn. CRC Press, Taylor & Francis Group, Boca Raton, pp 95–97
19. Brun LR, Brance ML, Lombarte M, Maher C, Di Loreto VE, Rigalli A (2015) Effects of yerba mate (*Ilex paraguariensis*) on histomorphometry, biomechanics, and densitometry on bones in the rat. *Calcif Tissue Int* 97:527–534 [PubMed: 26223790]
20. Parfitt AM, Drezner MK, Glorieux FH, Kanis JA, Malluche H, Meunier PJ, Ott SM, Recker RR (1987) Bone histomorphometry: standardization of nomenclature, symbols, and units. Report of the ASBMR Histomorphometry Nomenclature Committee. *J Bone Miner Res* 2:595–609 [PubMed: 3455637]
21. Harrar K, Hamami L (2012) An interconnectivity index for osteoporosis assessment using X-Ray images. *J Med Biol Eng* 33:569–575
22. Turner CH, Burr DB (1993) Basic biomechanical measurements of bone: a tutorial. *Bone* 14:595–608 [PubMed: 8274302]
23. Stürmer EK, Seidlová-Wuttke D, Sehmisch S, Rack T, Wille J, Frosch KH, Wuttke W, Stürmer KM (2006) Standardized bending and breaking test for the normal and osteoporotic metaphyseal tibias of the rat: effect of estradiol, testosterone, and raloxifene. *J Bone Miner Res* 21:89–96 [PubMed: 16355277]
24. R Development Core Team (2011) R: a language and environment for statistical computing R Foundation for Statistical Computing, Vienna, Austria ISBN 3–900051–07–0 <http://www.R-project.org/> Accessed 29 Nov 2016
25. Matkovi V, Kostial K, Simonovi I, Buzina R, Brodarec A, Nor-din BE (1979) Bone status and fractures in two regions of Yugoslavia. *Am J Clin Nutr* 32:540–549 [PubMed: 420146]
26. Bonjour JP, Carrie AL, Ferrari S, Clavien H, Slosman D, Theintz G, Rizzoli R (1997) Calcium-enriched foods and bone mass growth in prepubertal girls: a randomized, double-blind, placebo-controlled trial. *J Clin Invest* 99:1287–1294 [PubMed: 9077538]
27. Chan GM, Hoffman K, McMurry M (1994) Effect of dairy products on bone and body composition in pubertal girls. *Pediatrics* 126:551–556
28. Ruiz JC, Mandel C, Garabedian M (1995) Effect of spontaneous calcium intake and physical exercise on the vertebral and femoral bone mineral density of children and adolescents. *J Bone Min Res* 10:675–682
29. Lee WT, Leung SS, Leung DM, Tsang HS, Lau J, Cheng JC (1995) A randomized double blind controlled calcium supplementation and bone and height acquisition in children. *Br J Nutr* 74:125–139 [PubMed: 7547823]
30. Dibba B, Prentice A, Ceesay M, Stirling DM, Cole TJ, Poskitt EM (2000) Effect of calcium supplementation on bone mineral accretion in Gambian children accustomed to a low calcium diet. *Am J Clin Nutr* 71:544–549 [PubMed: 10648270]
31. Glastre C, Braillon P, David L, Cochat P, Meunier PJ, Delmas PD (1990) Measurements of bone mineral content of lumbar spine by dual X-ray absorptiometry in normal children: correlation with growth parameters. *J Clin Endocrinol Metab* 70:1330–1333 [PubMed: 2335574]
32. Welten DC, Kemper HC, Post GB, Van Mechelen W, Twisk J, Lips P, Teule GJ (1994) Weight bearing activity during youth is a more important factor for peak bone mass than calcium intake. *J Bone Min Res* 9:1089–1096
33. Sugimoto T, Kanatani M, Kano J, Kobayashi T, Yamaguchi T, Fukase M, Chihara K (1994) IGF-I mediates the stimulatory effect of high calcium concentration on osteoblastic cell proliferation. *Am J Physiol* 266:E709–E771 [PubMed: 8203509]
34. Allen LH, Oddoye EA, Margen S (1979) Protein-induced hyper-calciuria: a longer term study. *Am J Clin Nutr* 32:741–749 [PubMed: 433806]
35. Kerstetter JE, Kenny AM, Insogna KL (2011) Dietary protein and skeletal health: a review of recent human research. *Curr Opin Lipidol* 22:16–20 [PubMed: 21102327]

36. Kerstetter JE, Svastisalee CM, Caseria DM, Mitnick ME, Insogna KL (2000) A threshold for low-protein-diet-induced elevations in parathyroid hormone. *Am J Clin Nutr* 72:168–173 [PubMed: 10871576]

Author Manuscript

Author Manuscript

Author Manuscript

Author Manuscript

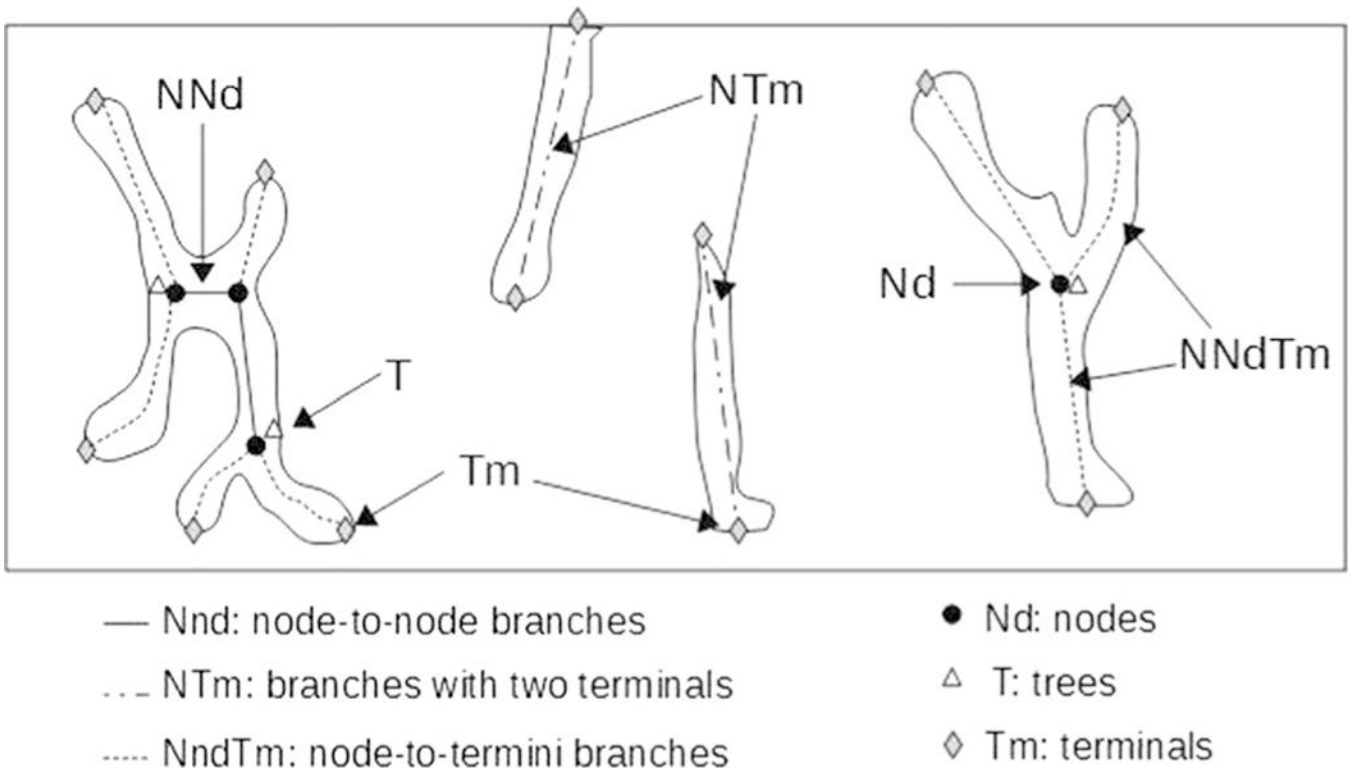


**Fig. 1.** Diagram of the skeletonized trabecular structure used in connectivity parameters measurement. The rectangle corresponds to a 0.6 mm<sup>2</sup> area at 0.1 mm from growth plate metaphyseal junction, the same anatomical location used for histomorphometric measurements

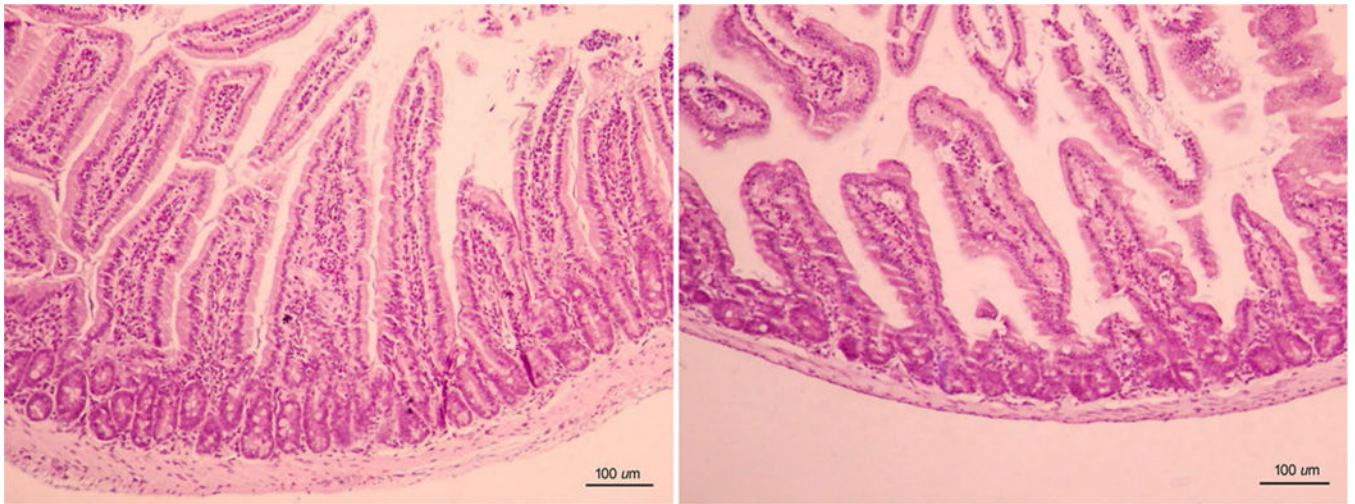


**Fig. 2.** Representative images of the duodenal tissue of WT mice ( $n = 7$ ) (left panel) and KO mice ( $n = 10$ ) (right panel). Left: Villi adopt a long finger-like projection covered by a columnar epithelium. The core of lamina propria is colonized specially with many immunocompetent cells. Right: In KO mice, villi presented shorter and broader, with a normal epithelium

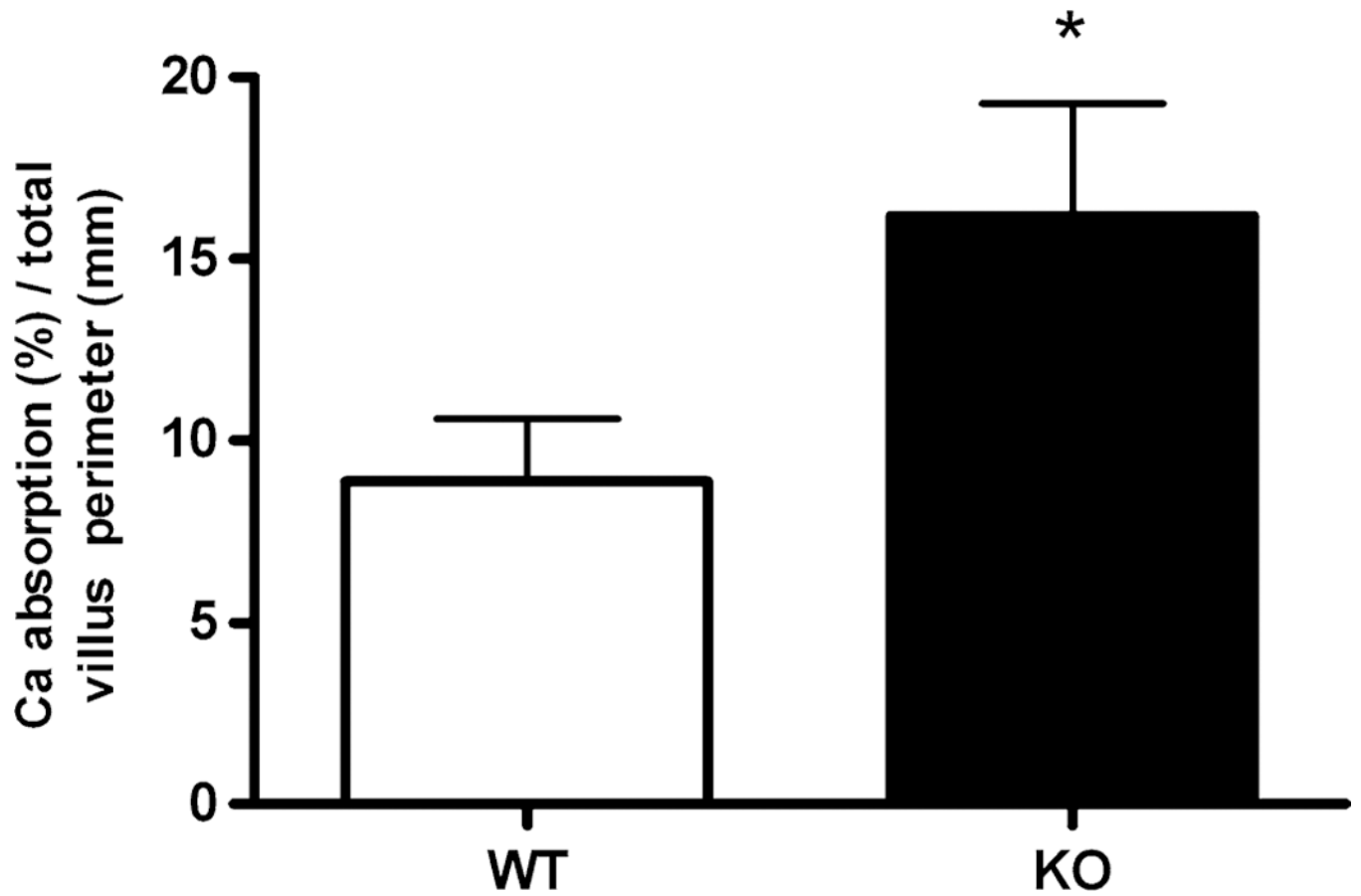


**Fig. 3.** Percentage of Ca uptake in WT ( $n = 7$ ) and KO ( $n = 10$ ) mice (\*significant differences versus WT mice,  $p < 0.05$ )

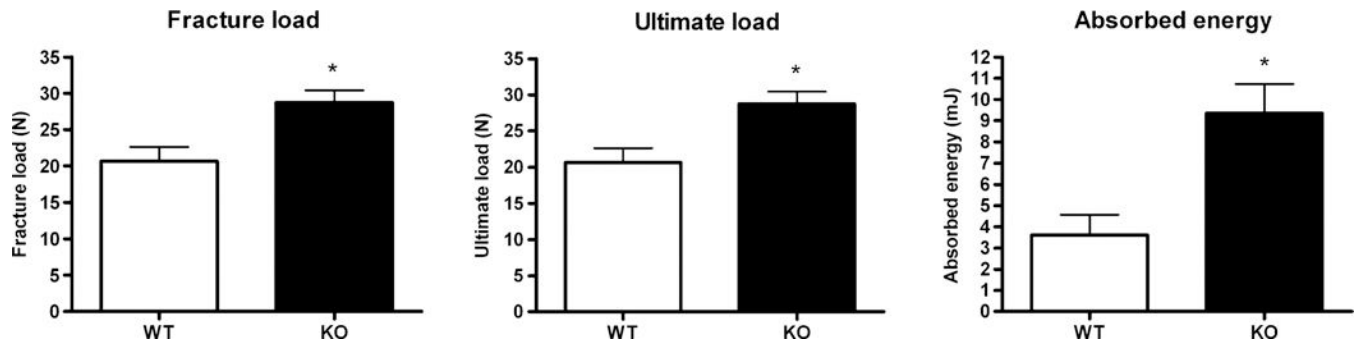


**Fig. 4.** Biomechanical parameters of femoral neck fracture test in WT ( $n = 7$ ) and KO ( $n = 10$ ) mice (\*significant differences versus WT mice,  $p < 0.05$ )

**Table 1**

In vivo Ca absorption, serum calcium and phosphate determinations

|                             | <b>WT (<i>n</i> = 7)</b> | <b>KO (<i>n</i> = 10)</b> |
|-----------------------------|--------------------------|---------------------------|
| Serum calcium (mg/dl)       | 8.31 ± 0.33              | 8.80 ± 0.20               |
| Serum phosphate (mg/dl)     | 3.45 ± 0.17              | 3.57 ± 0.39               |
| Urinary calcium (mg/24 h)   | 1.34 ± 0.23              | 1.74 ± 0.15               |
| Net Ca absorption (mg/24 h) | 5.99 ± 1.11              | 9.77 ± 2.26               |
| Ca retention (mg/24 h)      | 5.96 ± 0.86              | 8.11 ± 2.44               |

Author Manuscript

Author Manuscript

Author Manuscript

Author Manuscript

**Table 2**

## Duodenal villous and crypt morphometry

|                                      | WT ( <i>n</i> = 7) | KO ( <i>n</i> = 10) |
|--------------------------------------|--------------------|---------------------|
| Villus                               |                    |                     |
| Villus height (μm)                   | 445.9 ± 14.48      | 310.1 ± 19.3 *      |
| Villus diameter (μm)                 | 77.6 ± 2.5         | 93.4 ± 6.6 *        |
| Villus perimeter (mm)                | 1.14.0 ± 0.03      | 0.88 ± 0.49 *       |
| Total perimeter (mm)                 | 3.54 ± 0.13        | 2.65 ± 0.14 *       |
| Crypt                                |                    |                     |
| Crypt diameter (μm)                  | 41.2 ± 2.1         | 42.0 ± 1.5          |
| Area of the crypt (mm <sup>2</sup> ) | 12.05 ± 1.15       | 11.95 ± 078         |
| Area of cells (mm <sup>2</sup> )     | 10.85 ± 1.04       | 10.17 ± 0.73        |
| Height of the crypts cells (μm)      | 11.9 ± 0.6         | 11.6 ± 0.6          |

The “total perimeter” refers of the whole duodenal villus perimeter in each slide. Mean ± SEM (\*significant differences versus WT mice, Student’s *t* test, *p* < 0.05)

**Table 3**

## BMD and histomorphometry analysis

|                              | WT ( <i>n</i> = 7) | KO ( <i>n</i> = 10) |
|------------------------------|--------------------|---------------------|
| BMD (mg Ca/cm <sup>2</sup> ) | 10.47 ± 3.04       | 13.30 ± 1.54        |
| BV/TV (%)                    | 10.20 ± 1.25       | 14.58 ± 2.59        |
| Tb.Th (mm)                   | 0.029 ± 0.004      | 0.037 ± 0.005       |
| Tb.N (mm <sup>-1</sup> )     | 3.55 ± 0.36        | 3.85 ± 0.45         |
| Node-terminal ratio          | 0.17 ± 0.03        | 0.30 ± 0.03*        |
| ICI                          | 0.09 ± 0.05        | 0.18 ± 0.08         |
| NDX (%/mm)                   | 0.21 ± 0.13        | 1.53 ± 0.79         |
| NTm                          | 9.57 ± 2.51        | 4.78 ± 1.55*        |

Mean ± SEM (\*significant differences versus WT mice, Student's *t* test, *p* < 0.05)

Author Manuscript

Author Manuscript

Author Manuscript

Author Manuscript